Chemical Physics Letters 677 (2017) 80–86

Contents lists available at ScienceDirect

Chemical Physics Letters

journal homepage: www.elsevier.com/locate/cplett

Research paper

Role of oxygen functionality on the band structure evolution and conductance of reduced graphene oxide

Rajarshi Roy [a,d,2], Ranjit Thapa [b,2], Soubhik Chakrabarty [c], Arunava Jha [d,1], Priyanka R. Midya [d], E. Mathan Kumar [c], Kalyan K. Chattopadhyay [a,d,*]

[a] Thin Film and Nanoscience Laboratory, Dept. of Physics, Jadavpur University, Kolkata 700032, India
[b] SRM Research Institute & Department of Physics and Nanotechnology, SRM University, Kattankulathur 603203, Tamil Nadu, India
[c] Department of Materials Science, Indian Association for the Cultivation of Science, Jadavpur, Kolkata 700032, India
[d] School of Materials Science and Nanotechnology, Jadavpur University, Kolkata 700032, India

ARTICLE INFO

Article history:
Received 30 December 2016
In final form 28 March 2017
Available online 29 March 2017

Keywords:
Graphene oxide
Band structure
DFT
Transport

ABSTRACT

Here we report, structural and electrical transport properties of reduced graphene oxide as a function of oxygen bonding configuration. We find that mainly epoxy (C—O—C) and carbonyl (C=O) functional groups remain as major residual components after reduction using three different reducing agents. We calculate the band structure in the presence of epoxy and carbonyl groups and defects. Finally, we calculate the theoretical band mobility and find that it is less for the carbonyl with epoxy system. We correlate the distortion of linear dispersion and opening of bandgap at K-point with conductance for different graphene system in presence of oxygen moieties.

1. Introduction

Graphene has been the focal point of attention in materials science and nanotechnology since its discovery in 2004 [1]. It has proved itself to be a dream material for nanotechnologists over the years exhibiting all types of quantum electronic, optical and mechanical properties sandwiched in one single material [1–3]. Over the years the main challenge has been to tune the unique electronic properties of graphene into a tailor made configuration for specific device applications. However its poor yield hindered those applications, which needed bulk of the material and so the chemical analogue of graphene popularly known as 'Reduced graphene oxide (RGO)' has become popular in recent years [4]. It is to be noted that the bulk chemical synthesis mechanism of RGO gives away some of the important quantum relativistic electronic properties which is synonymous with monolayer graphene [1]. Therefore it is one material whose conductivity can greatly vary depending on different types of synthesis and reducing mechanisms involved [5–11]. The inherent structural attributes of RGO, regulates its electrical, thermal or mechanical behavior. For relatively defect free RGO, it can be highly conducting based on particle-to-particle interactions and known to show mostly p-type or ambi-polar conductance under suitable conditions [5,10]. To this end proper reduction of graphene oxide have been a much sort after field of research for many years to understand what percentage of sp^2 restoration character can be obtained and what would the possible reduced structure look like to achieve high conductivity but without compromising the bulk yield. Although there are many recent reports experimentally demonstrating the reduction of RGO from GO and predicting their structure through known experimental tools and conductivity measurements [5–13] but not much is known about their theoretical band structure evolution in presence of defects and oxygenated groups.

In this work we report prototype known reduction methods [5–9] of GO to RGO under three discrete reducing ambient [Hydrazine Hydrate and ammonia denoted as (HH), Sodium Borohydride ($NaBH_4$) with conc. Sulphuric acid denoted as (SBH-SA) and double conc. Sulphuric acid (SA-DC)]. This is followed by room temperature current-voltage measurements of the reduced RGO samples to analyze how the effect of residual oxygen functionalities and defects are influencing the conductance. Our analyses are also based upon previously known experimental tools to monitor the structural and compositional nature of the samples using Field emission scanning electron microscopy (FESEM), High-resolution transmission electron microscopy (HRTEM),

* Corresponding author at: Thin Film and Nanoscience Laboratory, Dept. of Physics, Jadavpur University, Kolkata 700032, India.
E-mail address: kalyan_chattopadhyay@yahoo.com (K.K. Chattopadhyay).
[1] Present address: St. Thomas' College of Engineering & Technology, 4 Diamond Harbour Road, Kolkata 700023, India.
[2] These authors contributed equally to the paper.

http://dx.doi.org/10.1016/j.cplett.2017.03.079
0009-2614/

X-ray Photoelectron Spectroscopy after reduction. Finally, we map the band structure evolution in RGO under different (oxygen moieties and defects) functionalities utilizing information from our experimental analysis and compare them with pristine graphene.

2. Experimental procedure

2.1. The preparation of graphite oxide by Hummer's method

Graphite oxide (GO) was synthesized by Hummer's method [14,15]. The starting materials are commercially available graphite powder (purchased from Sigma-Aldrich) (1 g), sodium nitrate (1 g) & potassium permanganate (6 g). Pure graphite & sodium nitrate were mixed with conc. sulphuric acid (46 ml) (98%) properly at room temperature and stirred for up to 10–15 min. Then, potassium permanganate ($KMnO_4$) was slowly added to the pre-treated solution while vigorous stirring for 1 h 20 min in ice bath. The temperature was kept near 0 °C while adding $KMnO_4$ to the mixture. The mixture was stirred for additional 1 h to mix the all precursors properly. The solution was then taken out from ice-bath and heated to 50–60 °C for 1 h 20 min without stirring followed by dilution with DI water (80 ml). Since addition of water in concentrated acid leads to large amount of heat release, the process was carried while all the effervescence from the mixture dissipated. The mixture was again stirred for 1 h and further diluted with 200 ml of DI water. After that, H_2O_2 (30%, 6 ml) was added to the mixture. Upon addition, the mixture turned yellow. After cooling down, the mixture was filtered and collected and then washed with DI water (200 ml) for removal of metal ions. The process was continued by repeated several times until the pH of the solution became neutral as the solution turned brown in texture. Finally the solution was exfoliated for 1 h with a 250 W horn sonicator followed by centrifugation for 10 min at 5000 rpm for proper exfoliation and the supernatant was collected.

2.2. Reduction of graphene oxide by hydrazine hydrate and ammonia (HH)

In this typical procedure at first 5 ml of exfoliated GO solution with 1 mg/ml loading was added to 5 ml of DI water in bath sonicator (40 W) until the solution is mixed properly. Then ammonium hydroxide (NH_4OH) (35 μL) & hydrazine hydrate (N_2H_4, $6H_2O$) (5 μL) (80%) were added to the pre-treated 10 ml GO solution &

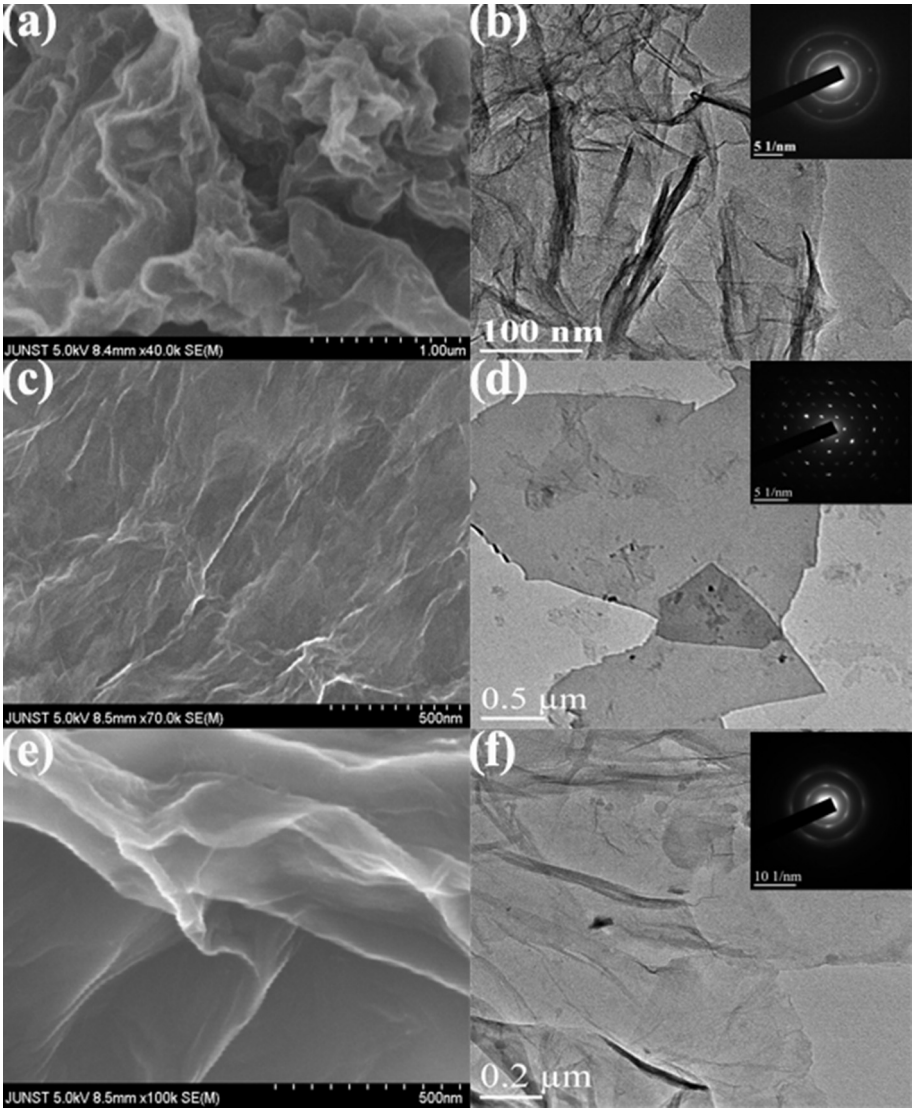

Fig. 1. FESEM and HRTEM images of the RGO samples reduced by (a and b) sodium borohydate and conc. Sulphuric acid (SBH-SA). (c and d) Hydrazine Hydrate and Ammonia (HH). (e and f) Double conc. sulphuric acid (SA-DC). The inset of (b, d, and f) show the hexagonal SAED pattern of the as prepared RGO samples.

stirred properly for 10–15 min at room temperature. Subsequently, the mixture was heated to 90 °C in water bath for 45mins under constant stirring. Eventually. The solution mixture turned to dark indicating reduction was completed. The final sample was collected and used for subsequent characterizations [5,8,9].

2.3. Reduction of graphene oxide by sodium borohydride and conc. sulphuric acid (SBH-SA)

This method consists of two-steps. At first reduction with sodium Borohydride ($NaBH_4$) with conc (21 mM) followed by dehydration with conc. sulphuric acid (H_2SO4) [6,9]. At first GO (100 mg) was mixed with 100 ml DI water properly and stirred at room temperature for 10–15 min. Then $NaBH_4$ was added slowly to the pre-treated solution and stirred for additional 20 min while the mixture was kept at 80 °C for 1 h with constant stirring. Eventually the product was filtered and washed with DI water for several times until the pH became 8–9. Then the solution was dried to obtain partially reduced GO. After this concentrated H_2SO_4 (100 ml) added to this collected partially reduced GO and stirred for 1 h to mix properly before refluxing for 12 h at 120 °C. Finally the product was collected and washed with DI water for several times to remove excess acids until the pH of the solution became neutral.

2.4. Reduction graphene oxide by double conc. sulphuric acid (SA-DC)

In this case aqueous sulfuric acid was used for the reduction of GO for the ring opening reaction. Graphene oxide (GO) (100 mg) was added to DI water (80 ml) and the mixture was put in bath sonicator for 10–15 min until the mixture was properly mixed. Then concentrated sulfuric acid [6] (98%) (5.56 ml) was added to sufficient DI water to make 1 M (100 ml) H_2SO_4 solution. The mixture was stirred at room temperature for 1 day. The product was collected. The product was partially reduced. Then the blackish product was filtered and washed with DI water. The pH was checked 6–7 for the partially reduced GO. The dehydration process is as follows. The dried product was dispersed in concentrated H_2SO_4 (100 ml) using bath sonicator for 1 h followed by refluxing for 12 h at 120 °C. The final product was dried and washed with DI water several times until the pH was neutral.

3. Results and discussion

From the FESEM images shown in Fig. 1, it was found that our as prepared samples consisted mostly of thin and wrinkled sheets, which lay over each other. In Fig. 1(a and c) the image showed the sample had more number of layers than the samples in Fig. 1 (b). This can be due to the variations in different degrees of exfoliation and reduction among the samples of different synthesized RGOs. In Fig. 1(d–f) the HRTEM images along with SAED in the insets for the synthesized RGOs are shown. Observable wrinkles and folded regions could be seen in the synthesized materials. The SAED (selected area electron diffraction) shown in the inset of the each figures, revealed ring-like six-fold hexagonal symmetry consistent with chemical graphene [13]. The sharp diffraction pattern for all the samples indicates to the presence of crystalline graphitic domains.

In Fig. 2(a) the Raman spectra of different RGOs as prepared and the GO sample are shown. All the spectra for the Raman bands (D, G) represent the distinctive features encountered for sp^2 carbon nano-structures. The G band is generally attributed to the E_{2g}

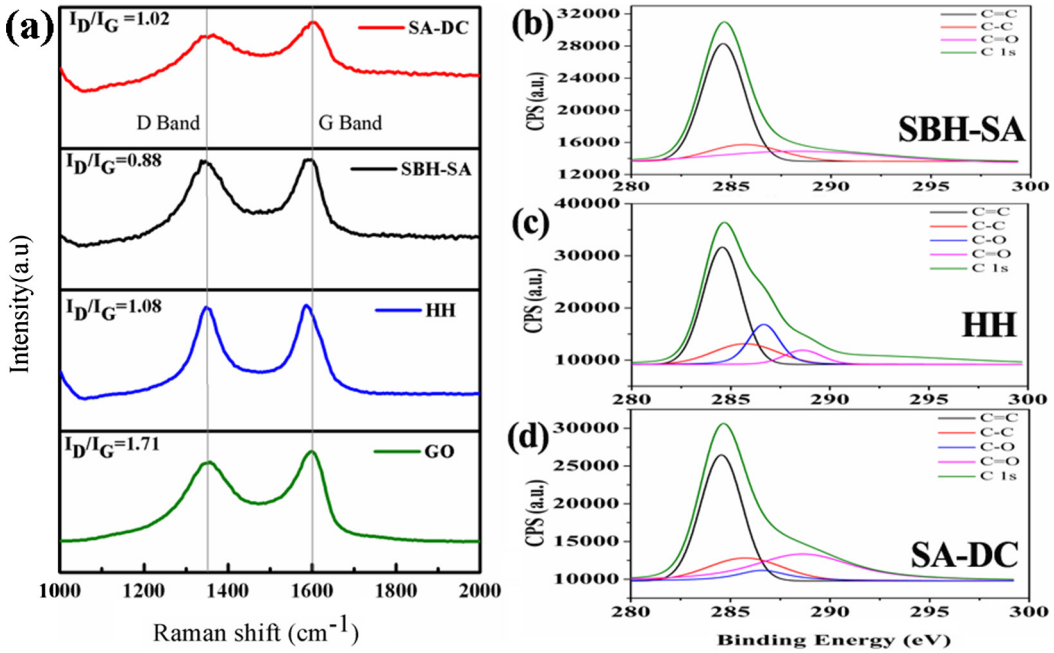

Fig. 2. (a) RAMAN spectra of different as prepared GO and RGOs samples. (b)–(d) XPS deconvoluted C1s spectra for RGO reduced with HH, SA-DC and SBH-SA respectively.

Table 1
Transport governing parameters of different RGO samples ascertained from experimental observations.

No.	Sample	Sheet resistance (MΩ/sq)	Expt. bandgap (eV)	I_D/I_G ratio	Defect density (cm^{-2})	L_a (nm)	C/O ratio
1	SBH-SA	0.0015	2.14	0.88	9.94×10^{10}	21.84	2.79
2	HH	2.74	2.73	1.08	1.22×10^{11}	17.8	1.65
3	SA-DC	1.5	2.52	1.02	1.15×10^{11}	18.84	1.99

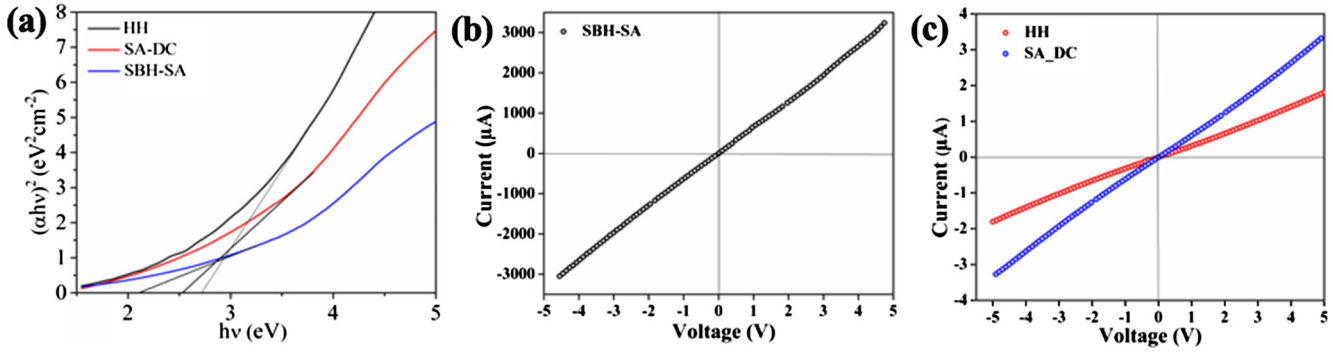

Fig. 3. (a) Calculated experimental band gap for all the RGO samples. I-V characteristics of RGO samples reduced in SBH-SA (b) HH and (c) SA-DC.

phonon of C sp^2 atoms, while the D band originates from a breathing k-point phonon with A_{1g} symmetry, which is related to local defects and disorders [13]. The intensity ratio between the two peaks (I_D/I_G) gives a measure of the aromaticity and restoration of graphitic domains from GO. A small change of the (I_D/I_G) ratio can indicate to the degree of 'graphitization' [13]. The intensity ratio (I_D/I_G) of RGOs reduced with SBH-SA, SA-DC & HH were found to be 0.88, 1.02 & 1.08 respectively. From the Raman shift it might be concluded that reduction level was varied for three RGO samples as prepared. The I_D/I_G ratio for the starting GO is found to be around 1.71. Now it is indeed observed that in some cases RGO reduction leads to increment of I_D/I_G ratio as reported by many research groups mainly [16,17]. However it is also seen that I_D/I_G ratio remained unchanged or decreased due to different reduction mechanisms [18,19]. As mentioned we have observed decrement of I_D/I_G ratio. Here, it is worth mentioning that we have considered peak area ratio of D and G bands respectively instead of amplitude ratio as we observe that our case the change in FWHM more than peak height change in some samples [20,21]. Furthermore, we calculate the defect density $n_D = 1.13 \times 10^{11}\left(\frac{I_D}{I_G}\right)$ for all the samples as shown in Table 1 and find that it is least corresponding to the SBH sample and highest for GO as D band scattering is proportional to the number of the point defect density and closely related to the I_D/I_G ratio [22]. We also calculate the nano-crystallite domain size (L_a) considering point defects, bond disorder, sp^2/sp^3 ratio, and so on in graphene by the formulation given by Cançado et al. $L_a = 2.4 \times 10^{-10}\lambda^4\left(\frac{I_D}{I_G}\right)^{-1}$, by considering λ = 532 nm and integrated peak area ratio instead of amplitude ratio as area ratio gives different results since FWHM(D) increases much more than FWHM(G) for decreasing L_a [20]. Upon calculating the crystallite size, it is found that it is least for GO at 11.24 nm and highest for the RGO reduced by SBH-SA at 21.84 nm as shown in Table 1. This observation of decrement in domain size from RGO to GO is also observed by Ganguly et al. [23]. The relative (I_D/I_G) is inversely proportional to the average domain size of the sp^2 clusters. As it is increased upon reduction, this confirms that new (or more) graphitic domains are formed and the sp^2 cluster number is increased after reduction in all the samples [17]. The main importance of the domain size and defect density is that both have a direct relationship with electrical conductance of these materials and their changes in carrier mobility [18]. Moreover we see that the G peak in GO is slightly blue shifted to higher wavenumber and is broader than its reduced counterparts suggesting significant oxidation. Red shifting of the G band with respect to GO as we observe distinctly in HH and SA-DC samples signifies the restoration of sp^2 carbon network in these samples [23].

Fig. 2(a–c) shows multiple deconvoluted regions of C1s spectra for RGOs reduced by SBH-SA, HH and SA-DC respectively. For sample SBH-SA, three distinct deconvoluted regions could be observed (Fig. 1a). The peak at 284.6 eV and 285.7 eV corresponds to C═C and C—C while the peak ~288.6 eV corresponds to C═O (carbonyl). There is no observable presence of C—O—C for this sample in our findings. However four distinctive peaks are observed after deconvolution is observed for RGO sample reduced by HH as shown in Fig. 1b. The peak at 284.7 eV and 285.7 eV arises due to the presence of C═C and C—C bonds as expected and further contributions of oxygen functional groups corresponds to peak ~286.6 eV for C—O—C (epoxy) and C═O (carbonyl) ~288.6 eV respectively [5,9–10,24,25]. For SA-DC, we observe the presence of C═C and C—C bonds at (284.5 eV) and (285.5 eV) respectively with additional oxygenated moieties from C—O—C (epoxy) (286.6 eV) and C═O (carbonyl) ~(288.6 eV) similar to the sample reduced by HH. In this context it must be mentioned that all the samples have been reduced well by their respective reducing agents as we have observed from our previous work [24] that unless GO is reduced well, the C1s shows a prominent doublet peak consisting of C═C/C—C and C—O bonds which wasn't observed here in any of the samples after reduction. Next we calculate the C:O ratio by considering C═C and C—C as a single entity factor in the numerator divided by the total contributing oxygenated species. We find that for HH the ratio is (1.65) and (1.99) for RGO reduced by SA-DC. But for SBH the ratio is quite large at (2.79) compared to the other samples because of considerably less presence of oxygenated bonds. Hence, it can be concluded that among the SBH acted as the reducing agent for rGO among all.

Fig. 3 demonstrates band gap and the I-V characteristics of all the RGO samples as prepared at room temperature. The calculated direct band gap for SBH-SA, SA-DC and HH and are found to be 2.14 eV, 2.52 eV and 2.73 eV. The I-V characteristics for all the samples are found to be ohmic in nature. The current rating for RGO reduced by HH and SA-DC is found to be very low (1–10 nA). However in case of RGO sample reduced by SBH-SA, a massive increment in current of the order of 10^3 is observed in comparison to other samples. We attribute this large increase in current due to high C/O ratio as mentioned earlier and signifies overall good reduction of RGO with SBH-SA as the reducing agent.

In the following section we have made an attempt to understand the conduction property of RGO using *ab initio* calculated band structures in presence of same type of residual oxygen functionalities as obtained from our experimental findings [26–28]. Optimized structures of the (5 × 5) supercell of graphene and corresponding band structures are estimated using the generalized gradient approximation (GGA) as implemented in *ab initio* approach, are shown in Fig. 3. The effect on band structures due to adsorbed epoxy (C—O—C) and carbonyl (C═O) group are analyzed in different combinations. To see the effect of C═O group on band structure of graphene, tri-vacancy defect has been intro-

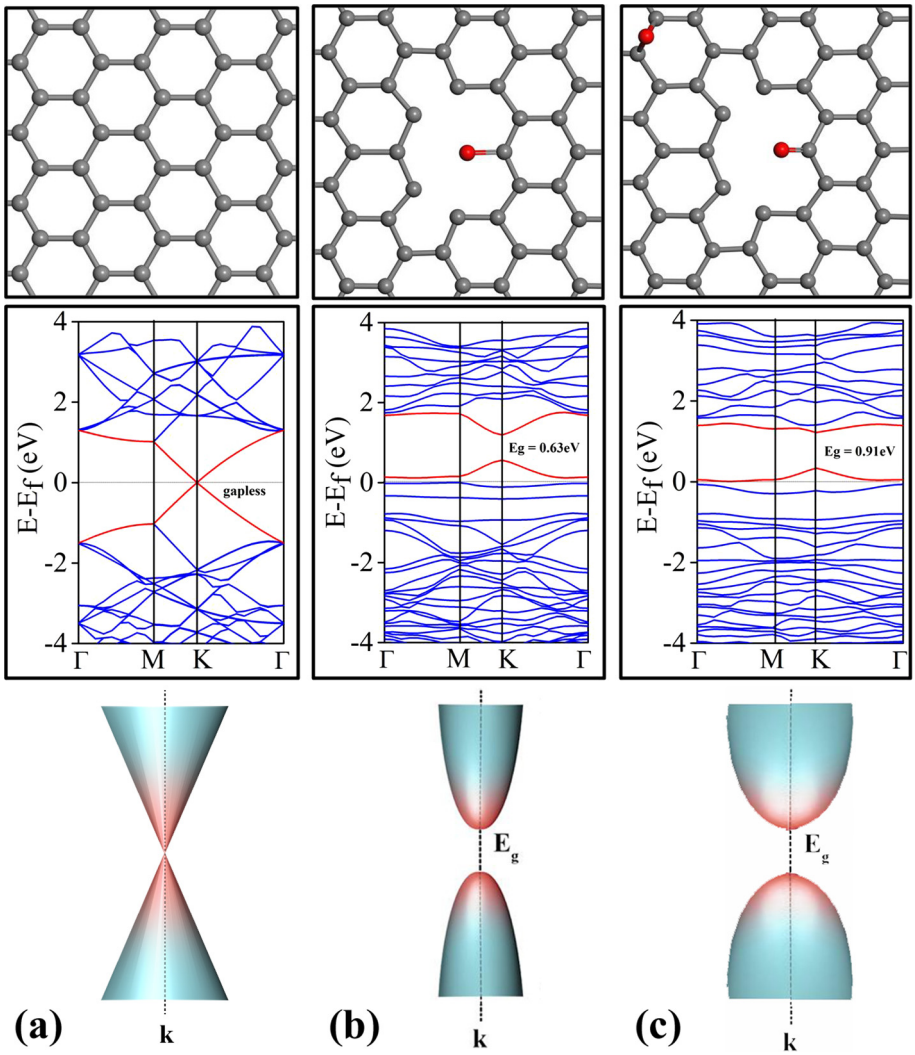

Fig. 4. Model, calculated band structure and schematic visualization of band dispersions around K-point of (a) (5 × 5) supercell of pure graphene (b) C=O over tri-vacancy graphene (RGO-1) and (c) C=O over tri-vacancy site with an adsorbed epoxy on the surface (RGO-2).

duced by removing the three C atoms from the main sp^2 bonded carbon sheet of graphene, and an oxygen atom is introduced to form bond with one of the carbon atom in the defect region. For C—O—C configuration, the oxygen atom has been placed on bridge site of two carbon atoms (A and B sublattice position) of the graphene sheet. The calculated binding energy of oxygen atom in C—O—C and C=O configuration are −2.3 eV and −3.1 eV respectively. The Mulliken charge at double bonded O atoms (0.54 e) is higher than the single bonded O atom (0.44 e), found to be the main reason of higher binding of C=O.

In Fig. 4(a) the band structure of pristine graphene is shown. As expected for graphene, a typical semi-metallic nature is observed following the linear relationship of energy with momentum at K-point. However the situation becomes more interesting when we introduce different types of oxygen adsorbates in the system (C—O—C, C=O) as added perturbations. The nature of the band dispersion near K point reveals fruitful information about conduction carrier mobility and concentration for graphitic system. First we took the examples of single bonded oxygen adsorbates over graphene surface, and performed band structure calculations. We have considered three different models of 2, 3 and 8 single bonded oxygen atoms to be adsorbed on bridge site of graphene sheet. In each of the cases we observe that the Fermi level position is within or just above the valence band thus proving the p-type nature with slight opening of band gap. The band gap increases slightly with increase in the number of single bonded oxygen atom from 2–3–8 (see Supplementary information, Fig. S1). However the most aspect to note is that how that band dispersions evolve around the K-point symmetry. It is seen that even after the opening of band gap, the linear nature of CBM (conduction band maxima) and VBM (Valence band minima) at K-point is maintained except for the 8 single bonded oxygen atom system where the bands at K-point are almost flat and linear dispersion relation is disrupted. We argue that this maintaining of the linear band dispersion at K point is directly related to carrier concentration and mobility of the material and thus affecting the conductance. For defected sheet (tri-vacancy only) we find that the linear dispersion nature is preserved at K-point, however the nature becomes much broader with increase in band gap with the attachment of single epoxy (see Supplementary information, Fig. S1). For only C=O (carbonyl) specie bonded over a tri-vacancy defected graphene sheet we find that the linear dispersion relationship around the K-point is broken as shown in Fig. 4(b). Here the CBM and VBM bands become broader and parabolic in nature with larger opening of band gap.

In Fig. 4(c) we address a more complex model and construct the supercell containing one C—O—C and one C=O over a defected graphene sheet to calculate the band structure. It is observed that the band gap has increased slightly from 0.63 eV to 0.81 eV with single addition of epoxy specie over the previous system (Fig. 4b) with considerably more flat parabolic band dispersion and broadening around K point, which can manifest to further decrement in conductance. We argue that the conductivity can change remarkably under minute band gap increment, and the nature of band dispersion around K-point plays a vital role. In such cases mobility and carrier concentration can be low in graphene like system if the linear band dispersion symmetry around K-point is broken.

To support our *ab initio* findings, we estimate the theoretical mobility for two structures (i) C=O (carbonyl) specie (SBH-SA analogue) present bonded over a tri-vacancy type defected graphene sheet denoted as RGO-1, and (ii) one C—O—C (epoxy) and one C=O (HH/SA-DC analogue) over a defected graphene sheet denoted as RGO-2, see Fig. 4b and c for the full optimized structure using a semi-classical parabolic approximation approach (Supplementary info) [28–31]. We obtain the carrier mobility of RGO-2, about $4.1 \times 10^4\,cm^2\,V^{-1}\,S^{-1}$ and $1.08 \times 10^5\,cm^2\,V^{-1}\,S^{-1}$ for the π and π^* band respectively. The carrier mobility of RGO-1, about $4.4 \times 10^4\,cm^2\,V^{-1}\,S^{-1}$ and $1.42 \times 10^5\,cm^2\,V^{-1}\,S^{-1}$ for the π and π^* band respectively. The results indicate that both for π and π^* band the carrier mobility of RGO-1 is higher than the RGO-2. This in turn also implies that conductivity (σ) will be better in RGO-1 (SBH-SA analogue) as it is directly proportional to mobility and proves to be consistent with our experimental findings.

In summary, we have carried out structural characterization and measured electrical I-V transport at room temperature for two as synthesized RGO samples using two separate reducing agents (Sodium borohydride with sulphuric acid, Double conc. sulphuric acid Hydrazine hydrate,). Henceforth we have conducted room temperature IV measurements and correlated the conductance with the presence of residual oxygen functionality present within the samples. Furthermore we have theoretically mapped the band structure evolution due to the presence of the different residual oxygen functionalities using *ab initio* analysis. Linear band dispersion is observed to be maintained for single epoxy attachment with slight opening of bandgap while band dispersion evolution from linear to parabolic is noticed as number of epoxy attachments increased from more than one with increase in bandgap. Parabolic to more parabolic flat band dispersion is observed with increase in band gap when surface functionality is changed from single carbonyl group on defected graphene sheet to a mixed functionality system with presence of both carbonyl with epoxy group in accordance with experimental results. This also affected the theoretical band mobility. We argue that the nature of band dispersion around K-point plays a pivotal role in governing conductivity of RGO due to changes in π-π^* band mobility in presence of various residual oxygen moieties and defects with minor change in bandgap.

Acknowledgment

One of the authors RR would like to thank and acknowledge the Council of Scientific and Industrial Research (CSIR), Government of India, for awarding him SRF fellowship during the tenure of this work. The authors would also like to thank the UGC for 'University with potential for excellence scheme (UPEII)' and the DST, the Government of India for financial support. RT thanks SRM University for providing supercomputing facility and financial support.

Appendix A. Supplementary material

Characterization details, *ab-initio* band structures with single and multiple epoxy group presence on graphene surface and details of theoretical mobility calculations. Supplementary data associated with this article can be found, in the online version, at http://dx.doi.org/10.1016/j.cplett.2017.03.079.

References

[1] A.K. Geim, Graphene: status and prospects, Science 19 (2009) 1530–1534.
[2] A.K. Geim, K.S. Novoselov, The rise of graphene, Nat. Mater. 6 (2007) 183–191.
[3] F. Schwierz, Graphene transistors, Nat. Nanotechnol. 5 (2010) 487–496.
[4] O.C. Compton, S.B.T. Nguyen, Graphene oxide, highly reduced graphene oxide, and graphene: versatile building blocks for carbon-based materials, Small 6 (2010) 711–723.
[5] S. Stankovich, D.A. Dikin, R. Piner, K.M. Kohlhaas, A. Kleinhammes, Y. Jia, Y. Wu, S.T. Nguyen, R.S. Ruoff, Synthesis of graphene-based nanosheets via chemical reduction of exfoliated graphite oxide, Carbon 45 (2007) 1558–1565.
[6] D. Kim, S.J. Yang, Y.S. Kim, H. Jung, C.R. Park, Simple and cost-effective reduction of graphite oxide by sulfuric acid, Carbon 50 (2012) 3229–3232.
[7] S. Park, J. An, J.R. Potts, A. Velamakanni, S. Murali, R.S. Ruoff, Hydrazine-reduction of graphite-and graphene oxide, Carbon 49 (2011) 3019–3023.
[8] D. Li, M.B. Muller, S. Gilje, R.B. Kaner, G.G. Wallace, Processable aqueous dispersions of graphene nanosheets, Nat. Nanotechnol. 3 (2008) 101–105.
[9] H.J. Shin, K.K. Kim, A. Benayad, S.M. Yoon, H.K. Park, I.S. Jung, M.H. Jin, H.K. Jeong, J.M. Kim, J.Y. Choi, Y.H. Lee, Efficient reduction of graphite oxide by sodium borohydride and its effect on electrical conductance, Adv. Func. Mater. 19 (19) (2009) 1987–1992.
[10] P.G. Ren, D.X. Yan, X. Ji, T. Chen, Z.M. Li, Nanotechnology 22 (2011) 055705.
[11] S. Some, Y. Kim, Y. Yoon, H. Yoo, S. Lee, Y. Park, H. Lee, High-quality reduced graphene oxide by a dual-function chemical reduction and healing process, Sci. Rep. 3 (2013) 1929.
[12] C. Gómez-Navarro, R.T. Weitz, A.M. Bittner, M. Scolari, A. Mews, M. Burghard, K. Kern, Electronic transport properties of individual chemically reduced graphene oxide sheets, Nano Lett. 9 (2009) 2206.
[13] C. Mattevi, G. Eda, S. Agnoli, S. Miller, K. Andre Mkhoyan, O. Celik, D. Mastrogiovanni, G. Granozzi, E. Garfunkel, M. Chhowalla, Evolution of electrical, chemical, and structural properties of transparent and conducting chemically derived graphene thin films, Adv. Func. Mater. 19 (2009) 2577–2583.
[14] L.J. Cote, F. Kim, J. Huang, Langmuir Blodgett assembly of graphite oxide single layers, J. Am. Chem. Soc. 131 (2009) 1043–1049.
[15] W.S. Hummers, R.E. Offeman, Preparation of graphitic oxide, J. Am. Chem. Soc. 80 (1958) 1339.
[16] A.A. Dubale, W.-N. Su, A.G. Tamirat, C.-J. Pan, B.A. Aragaw, H.-M. Chen, B.-J. Hwang, Synergetic effect of graphene on Cu_2O nanowire arrays as highly efficient hydrogen evolution photocathode in water splitting, J. Mater. Chem. A 2 (2014) 18383–18397;
A. Ambrosi, A. Bonanni, Z. Sofer, J.S. Cross, M. Pumera, Electrochemistry at chemically modified graphenes, Chem. Eur. J. 17 (2011) 10763–10770.
[17] G. Sobon, J. Sotor, J. Jagiello, R. Kozinski, M. Zdrojek, M. Holdynski, P. Paletko, J. Boguslawski, L. Lipinska, K.M. Abramski, Graphene oxide vs. reduced graphene oxide as saturable absorbers for Er-doped passively mode-locked fiber laser, Opt. Express 20 (2012) 19463–19473.
[18] Goki Eda, Manish Chhowalla, Chemically derived graphene oxide: towards large-area thin-film electronics and optoelectronics, Adv. Mater. 22 (2010) 2392–2415.
[19] V. Lee, L. Whittaker, C. Jaye, K. Baroudi, D.A. Fischer, S. Banerjee, Large-area chemically modified graphene films: electrophoretic deposition and characterization by soft X-ray absorption spectroscopy, Chem. Mater. 21 (2009) 3905–3916.
[20] Andrea C. Ferrari, Raman spectroscopy of graphene and graphite: disorder, electron–phonon coupling, doping and nonadiabatic effects, Solid State Commun. 143 (2007) 47–57.
[21] L.G. Cançado, K. Takai, T. Enoki, M. Endo, Y.A. Kim, et al., General equation for the determination of the crystallite size La of nanographite by Raman spectroscopy, Appl. Phys. Lett. 88 (2006) 163106.
[22] S. Gupta, E. Heintzman, J. Jasinski, Nanocarbon hybrids of graphene-based materials and ultradispersed diamond: investigating structure and hierarchical defects evolution with electron-beam irradiation, J. Raman Spectrosc. 46 (2015) 509–523.
[23] Abhijit Ganguly, Surbhi Sharma, Pagona Papakonstantinou, Jeremy Hamilton, Probing the thermal deoxygenation of graphene oxide using high-resolution in situ X-ray-based spectroscopies, J. Phys. Chem. C 115 (2011) 17009–17019.
[24] U.N. Maiti, S. Maiti, T.P. Majumder, K.K. Chattopadhyay, Ultra-thin graphene edges at the nanowire tips: a cascade cold cathode with two-stage field amplification, Nanotechnology 22 (2011) 505703.
[25] R. Roy, A. Jha, D. Sen, D. Banerjee, K.K. Chattopadhyay, Unique quasi-vertical alignment of RGO sheets under an applied non-uniform DC electric field for enhanced field emission, J. Mater. Chem. C 36 (2014) 7608–7613.

[26] M.D. Segall, P.J.D. Lindan, M.J. Probert, C.J. Pickard, P.J. Hasnip, S.J. Clark, M.C. Payne, First-principles simulation: ideas, illustrations and the CASTEP code, J. Phys.: Condens. Matter 14 (2012) 2717–2744.
[27] D. Vanderbilt, Soft self-consistent pseudopotentials in a generalized eigenvalue formalism, Phys. Rev. B 41 (1990) 7892–7895.
[28] J.P. Perdew, K. Burke, M. Ernzerhof, Generalized gradient approximation made simple, Phys. Rev. Lett. 77 (1996) 3865–3868.
[29] S. Bruzzone, G. Fiori, Ab-initio simulations of deformation potentials and electron mobility in chemically modified graphene and two-dimensional hexagonal boron-nitride, Appl. Phys. Lett. 99 (2011) 2108.
[30] S. Takagi, A. Toriumi, M. Iwase, H. Tango, On the universality of inversion layer mobility in Si MOSFET's: Part I-effects of substrate impurity concentration, IEEE Trans. Electron. Devices 41 (1994) 2357–2362.
[31] J. Bardeen, W. Shockley, Deformation potentials and mobilities in non-polar crystals, Phys. Rev. 80 (1950) 72–80.